Journal of Catalysis 274 (2010) 150–162

Contents lists available at ScienceDirect

Journal of Catalysis

journal homepage: www.elsevier.com/locate/jcat

An investigation into the mechanism and kinetics of dimethoxymethane carbonylation over FAU and MFI zeolites

Fuat E. Celik, Taejin Kim, Anton N. Mlinar, Alexis T. Bell *

Department of Chemical Engineering, University of California, Berkeley, CA 94720, USA

ARTICLE INFO

Article history:
Received 24 May 2010
Revised 22 June 2010
Accepted 24 June 2010
Available online 2 August 2010

Keywords:
Carbonylation
Acid
Zeolite
FTIR
Infrared
Faujasite
Carbon monoxide
Dimethoxymethane
Methyl methoxyacetate
Disproportionation

ABSTRACT

In situ IR spectroscopy was used to observe the intermediates formed on zeolites FAU and MFI during the synthesis of methyl methoxyacetate (MMAc) via carbonylation of dimethoxymethane (DMM) and the disproportionation of DMM to dimethyl ether (DME) and methyl formate (MF). Both reactions are initiated by the reaction of DMM with the Brønsted acid protons of the zeolite to form methanol and methoxymethoxy groups (MMZ). The latter species then undergoes one of two processes – carbonylation to form methoxyacetyl species, the precursors to MMAc, or reaction with DMM, resulting in DMM disproportionation. Surface intermediates for both DMM carbonylation and disproportionation respond to changes in reaction conditions in a manner consistent with observed steady-state kinetics. DMM carbonylation occurred more rapidly in the presence than absence of physisorbed DMM, a phenomenon attributed to solvation of the carbocationic transition state involved in the addition of CO to MMZ predicted by DFT calculations. The surface concentration of the methoxyacetyl species at steady state was 10 times smaller on FAU than on MFI, consistent with the higher rate of DMM carbonylation on FAU. Rate expressions for the formation of each product, based on the proposed mechanisms, in combination with a suitable set of rate coefficients, give a good description of the experimentally observed dependences of the rates of product formation on temperature and the feed partial pressures of CO and DMM.

1. Introduction

Monoethylene glycol (MEG) is a commodity chemical widely used as antifreeze and as a monomer in the synthesis of polyester fibers. The current production of MEG is by epoxidation of ethylene and subsequent hydration of the resulting ethylene oxide [1]. While this technology is highly developed, the rising cost of ethylene derived from petroleum or natural gas has motivated consideration of alternative routes. The lower cost of carbon derived from synthesis gas (CO and H_2), produced by gasification of coal or other low hydrogen content feed stocks, relative to that derived from ethylene, has led to an interest in identifying routes to MEG from synthesis gas. While the direct production of MEG from synthesis gas has been investigated, such processes suffer from low yields and require very high pressures (1300–7000 atm) [2,3]. An alternate approach to forming MEG from synthesis gas is to begin with methanol, which can then oxidized to obtain formaldehyde or its dimethyl acetal, dimethoxymethane (DMM) [4,5]. Since these are C_1 compounds lacking a C—C bond, they can be converted to C_2 compounds by carbonylation. Several attempts to carry out the acid-catalyzed carbonylation of formaldehyde in the liquid-phase have been reported [6–9], with efforts being made to achieve high selectivity at low pressure [10–12]. However, the rate of formaldehyde carbonylation in all cases has been limited by the low solubility of CO in the solvent used, which results in poor selectivity for reactions carried out at low pressures due to the reactivity of the formaldehyde [12].

We have recently shown that the vapor-phase carbonylation of DMM can catalyzed by acidic zeolites [13,14]. The product of DMM carbonylation is methyl methoxyacetate (MMAc), which can then be converted to MEG in two steps. In the first step, MMAc is hydrogenated to ethylene glycol monomethyl ether, and in the second step, this intermediate is hydrolyzed to produce MEG. Using FAU, 79% selectivity to MMAc was achieved at 393 K and a total pressure of 3 atm [13]. DMM disproportionation, which produces dimethyl ether (DME) and methyl formate (MF), was the only side-reaction, in contrast to liquid-phase reactions, which produced a large number of by-products [7,9,12]. The highest selectivity to MMAc was achieved with FAU, whereas smaller pore zeolites such as MFI, BEA, MOR, and FER were significantly less selective. MMAc formation rates increased with increasing CO partial pressure and were nearly independent of DMM partial pressure over both MFI and FAU. Both catalysts exhibited a maximum MMAc formation rate as a function of reaction temperature, whereas DMM disproportionation rates increased monotonically

* Corresponding author. Fax: +1 510 642 4778.
E-mail address: bell@cchem.berkeley.edu (A.T. Bell).

0021-9517/$ - see front matter © 2010 Elsevier Inc. All rights reserved.
doi:10.1016/j.jcat.2010.06.015

with temperature. DMM disproportionation rates increased with increasing DMM partial pressure and were independent of CO partial pressure on FAU. The activity of MFI for DMM disproportionation was severely inhibited by the presence of CO [14]. Attainment of high MMAc selectivity required a high ratio of CO/DMM partial pressures and a low DMM partial pressure (~0.01–0.02 atm).

The aim of present study is to provide evidence for the mechanism proposed in our earlier work [14] and to identify the factors limiting the rates of reaction and effecting the activity and selectivity of the catalysts. In situ FTIR spectroscopy was used to identify reaction intermediates and to probe key elementary processes involved in the carbonylation of DMM to MMAc. The spectroscopic evidence supports our proposed mechanism and is consistent with steady-state rate data that we reported earlier [14] and with an analysis of the proposed mechanism using density functional theory [15]. Rate expressions derived from the proposed mechanism provide an accurate description of the dependences of the rates of MMAc, DME, and MF formation on temperature and feed partial pressures of CO and DMM observed experimentally.

2. Experimental

2.1. Catalyst preparation

H-FAU with Si/Al ratio ≈30 was obtained from Zeolyst and Na-MFI with Si/Al ≈ 27.5 was obtained from Süd-Chemie. Na-ZSM was converted to the NH_4^+-form by aqueous exchange with 1 M NH_4NO_3 solution. Five grams of Na-MFI was exchanged with 0.1 L of solution for 12 h at 353 K three times, filtering, and washing with 0.1 L deionized water each time. After the final exchange, the sample was filtered and rinsed again and dried at 383 K for 36 h. Removal of residual moisture and conversion to the H^+ form was achieved by heating to 773 K for 3 h at the rate of 2 K min^{-1} in 100 cm^3 min^{-1} flow of dry air (zero-grade). Residual moisture was removed from H-FAU by treatment in dry air for 3 h at 773 K as described above.

High-surface area SiO_2 (MCM-41) was prepared according to established techniques [16] with a surface area of 1106 m^2 g^{-1} (as determined by N_2 adsorption). Prior to use, the SiO_2 was heated to 773 K at 4 K min^{-1} and held for 1 h.

2.2. Collection of FTIR spectra

Infrared spectra were acquired using a Thermo Scientific Nicolet 6700 FTIR spectrometer equipped with a liquid nitrogen-cooled MCT detector. Each spectrum was obtained by averaging 32 scans taken with 1 cm^{-1} resolution. Catalysts were pressed into 20-mm-diameter pellets (<1 mm thick) and placed into a custom-built transmission cell equipped with CaF_2 windows, a K-type thermocouple for temperature control, and resistive cartridge heaters similar to that described in [17]. All pressed pellets were heated to 773 K with ramp rates and durations listed above in the transmission cell prior to the introduction of adsorbate gases. All scans were acquired at 383 K. Experiments at elevated pressure were carried out by throttling a needle valve located downstream from the reactor. Unless otherwise noted, the total gas flow rate through the reactor was maintained at 100 cm^3 min^{-1}, meaning that at elevated pressures, the gas flow rate exceeded 100 cm^3 min^{-1} at STP. Gases used included CO (99.99% pure research grade, Praxair), DMM (9.96% in He, Praxair), MF (9.94% in He, Praxair), DME (99.5% chemically pure, Praxair), He (99.999% ultra-high purity, Praxair), and 3.99% DMM in CO (Praxair). Pure CO was supplied in a steel cylinder, leading to the formation of iron pentacarbonyl [18]. A trap packed with 3.2-mm pellets of 3A molecular sieve was placed in the CO gas line to remove the iron pentacarbonyl.

All absorption spectra were taken relative to the empty transmission cell. In addition, spectra above 3160 cm^{-1} were baseline corrected and spectra below 3060 cm^{-1} were baseline corrected after subtracting the spectrum of the bare support (FAU, MFI, or SiO_2).

2.3. Steady-state and transient-response rate data

Rate measurements were taken in a 6.35-mm OD quartz tube reactor with an expanded section (~12.7 mm OD, ~20 mm length). The reactor was packed with quartz wool above and below the catalyst bed to hold the catalyst powder in place. The reactor was placed inside a resistively heated ceramic furnace with external temperature control, and the catalyst bed temperature was measured with a K-type thermocouple sheathed in a quartz capillary placed in direct contact with the bed. Reaction products were analyzed using an Agilent 6890 N gas chromatograph equipped with a bonded polystyrene–divinylbenzene (HP-PLOT Q) capillary column connected to a flame ionization detector and an MKS Mini-Lab quadrupole mass spectrometer. Reaction conditions were chosen to reproduce the conditions in the transmission IR cell.

3. Results and discussion

3.1. FTIR spectra of DMM and DMM-like adsorbed species

The spectrum of physically adsorbed DMM physisorbed on SiO_2 was acquired in the following manner. High-surface area SiO_2 was saturated under a flow rate of 100 cm^3 min^{-1} of 0.01 atm DMM in He at 383 K. Table 1 lists the IR bands observed in this experiment

Table 1
Comparison of vibrational frequencies in DMM and DMM-like species at 383 K (cm^{-1}).

DMM vapor	DMM/SiO_2 flowing 0.01 atm DMM in He	DMM/FAU flowing 0.01 atm DMM in He	DMM/FAU flowing He	Band assignments[a]
3004 m	3006 m	3005* w 2995* m	3003* w 2995* w 2982* w	a-ν CH_3 a-ν CH_3
2942 m	2960* m	2955* m	2962 s	a-ν CH_2, ν CH_3, 2δ CH_3
2936 s	2946 s	2946 s	2946* w	s-ν CH_3, a-ν CH_2, 2δ CH_3
2901* m	2898 m	2910 s	2912 s	s-ν CH_2
2853 w	2850* w	2855* w	2858 s	Unassigned
2838 m	2838 m	2836 s 2802 w	2839 m 2802 m	s-ν CH_3
2774 w	2782 w	2780 w		Unassigned
1755				
		1734	1734	
		1490* w	1490 m	
1472 w	1477 w	1475* w	1475* w	δ CH_2 scissoring
1467* w	1467 w	1467 m	1467* w 1458 s	s-δ CH_3
1456 s	1453 s	1450 s 1435 w	1450 m 1435* w 1417 m	a-δ CH_3
1398 s	1403 s	1400 s	1400 m	δ CH_2 wagging
		1385* w	1385* w	

ν stretching vibration, δ deformation vibration, s symmetric, a asymmetric.
s strong, m moderate, w weak relative to bands within same region of spectrum.
* Frequency estimated from a peak shoulder.
[a] Band assignments based on DMM vapor [19].

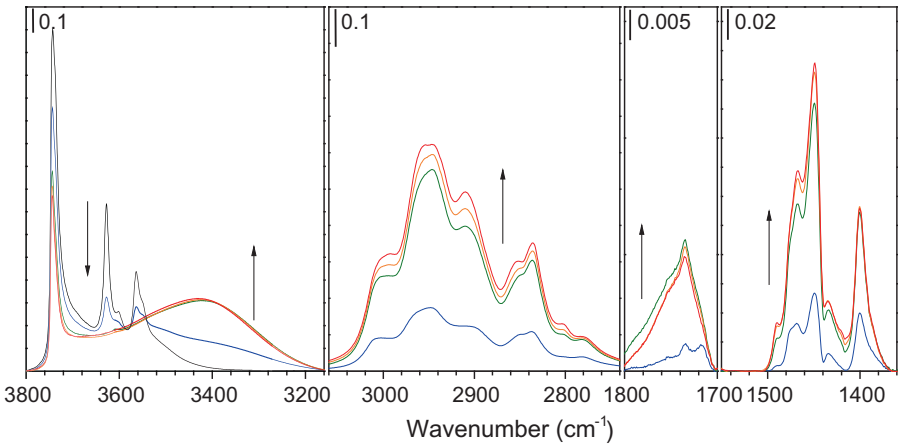

Fig. 1. IR spectra recorded during transient-response experiments of H-FAU exposed to 0.01 atm DMM. Black: 0 s, blue 45 s, green 90 s, orange 271 s, red 996 s. 0.0479 g catalyst, 383 K, 100 cm^3 min^{-1} at 1 atm. (For interpretation of the references to colour in this figure legend, the reader is referred to the web version of this article.)

and compares them with those for gas-phase DMM [19]. A one-to-one correlation of C—H stretching- and bending-vibrations between vapor-phase DMM and DMM adsorbed on SiO_2 at 383 K is seen, indicating that DMM physisorbs on SiO_2 intact. Certain modes for physisorbed DMM (asymmetric CH_2 stretching, symmetric CH_3 stretching, and an unassigned band shifting from 2774 cm^{-1} to 2782 cm^{-1}) appear at higher frequencies than seen in the gas-phase spectrum of DMM, due likely to dispersive interaction of the physisorbed molecule with the SiO_2. Upon switching the gas flow to pure He, all C—H vibrations rapidly disappeared, indicating that only physisorbed species were present. Table 1 also shows that the spectrum of DMM interacting with FAU taken at 383 K is very similar to that for SiO_2, indicating that the spectrum is dominated by physisorbed DMM.

The spectrum of H-FAU (Fig. 1, black curve), taken prior to exposure of the zeolite to DMM, exhibits a peak at 3744 cm^{-1} due to silanol groups associated with external, lattice-terminating defects and internal SiOH nests associated with defect groups generated upon dealumination of the zeolite [20,21]. In FAU samples with high Si/Al ratios, the contribution to the silanol peak from internal nested defects is significant because FAU is synthesized with a Si/Al ratio ≈2.6 and then dealuminated to give the desired Si/Al ratio [22]. The large peak at 3744 cm^{-1} observed for H-FAU with Si/Al ≈ 30 is the result of significant zeolite dealumination. The peaks at 3628 and 3564 cm^{-1} are due to Brønsted acidic protons associated with O(1) sites located in the FAU supercages and O(3) sites located in the sodalite cages [20,21,23]. The shoulder at 3550 cm^{-1} is unassigned but may be due to protons at the O(2) sites that point into the hexagonal prisms of FAU. The peak at 3602 cm^{-1} is assigned to extra-framework aluminum species (EFAL) [20,21]. The low intensity of this peak, coupled with the lack of a peak at ~3695 cm^{-1}, indicates the sample has a very low EFAL content.

The interactions of DMM with H-FAU (Si/Al ≈ 30) were characterized in the following manner. The zeolite was first exposed to flow of 100 cm^3 min^{-1} of 0.01 atm DMM in He at 383 K. IR spectra were acquired for about 1000 s, at which point they no longer changed with time. Upon exposure to DMM (Fig. 1), the O—H stretching vibrations associated with both Brønsted acidic sites and non-acidic SiOH groups decreased, while a broad feature around 3430 cm^{-1} grew concurrently with the growth in the C—H stretching (2740–3060 cm^{-1}) and C—H deformation vibrations (1360–1500 cm^{-1}) associated with physisorbed species. The broad peak at 3430 cm^{-1} is attributed to hydrogen bonding of DMM with O—H groups on the zeolite surface, which causes a bathochromic shift in all of the O—H stretching vibrations. After 90 s of DMM exposure, all of the Brønsted acidic O—H groups were covered by either physically or chemically adsorbed DMM molecules, resulting in a disappearance of both the high- and low-frequency bands.

The steady-state spectrum of FAU taken in flowing DMM (Fig. 1, red[1] and Fig. 2, black) is similar to that of DMM physisorbed on SiO_2. All of the peaks of physisorbed DMM are observed with only small shifts in frequency. During the approach to steady state, the band assigned primarily to asymmetric CH_2 stretching vibrations (2955 cm^{-1}) grew more slowly but reached a greater intensity than the adjacent band assigned primarily to symmetric CH_3 stretching vibrations (2946 cm^{-1}). Similarly, the symmetric CH_2 stretching band at 2910 cm^{-1} grew more slowly than the symmetric CH_3 stretching band at 2836 cm^{-1}. The slower growth rate of bands associated with CH_2 groups relative to CH_3 groups indicates that the CH_2/CH_3 ratio in the surface species increased with time from an initially low value.

After ~1000 s of DMM exposure, the sample was flushed with He to remove gaseous and physisorbed species (Fig. 2), leaving only chemisorbed species. The C—H stretching vibration peaks associated with CH_2 groups (2962 cm^{-1} and 2910 cm^{-1}) decreased in intensity less than those associated with CH_3 (2995–3003 cm^{-1}, 2946 cm^{-1}, and 2836 cm^{-1}), such that the relative intensities of peaks for CH_2 groups were larger than those for CH_3 groups. It was also observed that as physisorbed DMM was removed from the IR cell, the intensities of both the silanol groups and Brønsted acidic groups increased.

Fig. 3 shows the proposed physical and chemical adsorption modes of DMM at a zeolite Brønsted acid site. Hydrogen-bonded physisorbed DMM possesses a CH_2/CH_3 ratio of 0.5, identical to gas-phase DMM. Physisorbed DMM is envisioned to undergo protonation with the loss of methanol and the formation of methoxy-methoxy species (MMZ). Two experimental observations support the occurrence of this process. The first is the observation by mass spectrometry of a burst of methanol when the zeolite is first contacted with DMM, as shown in Fig. 4. A small amount of water is also observed, which is attributed to the dehydration of methanol to form DME. DME formation was also observed, but as disproportionation was also occurring, the DME formed cannot be solely attributed to the displacement of protons. The total number of protons displaced in 600 s is equivalent to 53% of the Brønsted acidic protons in the sample. The remaining protons were likely associated with physisorbed DMM. Prolonged flushing of physisorbed

[1] For interpretation of color in Figs. 1, 2, 6–15 the reader is referred to the web version of this article.

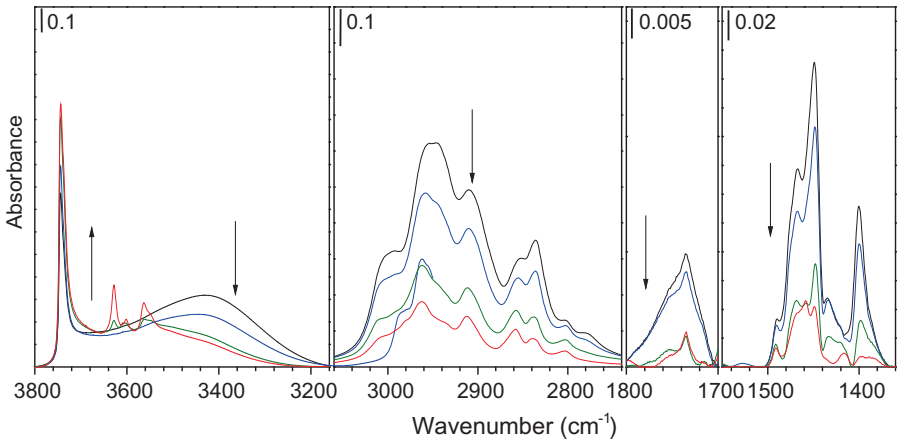

Fig. 2. IR spectra recorded during transient-response experiments of FAU under He flow following exposure to 0.01 atm DMM/He. Black 0 s, blue 46 s, green 765 s, red 4508 s. 0.0479 g catalyst, 383 K, 100 cm^3 min^{-1} at 1 atm.

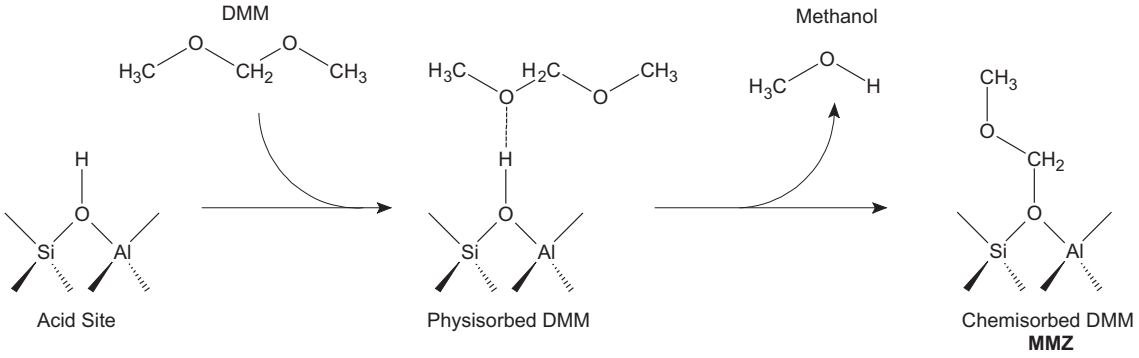

Fig. 3. Physical and chemical modes of DMM adsorption at Brønsted acid site of a zeolite.

DMM with He (Fig. 2) showed the regeneration of roughly half of the original IR peak intensity for Brønsted acidic OH groups, providing further evidence that half the Brønsted acid sited had reacted with DMM to form MMZ and other surface species. Further evidence for the formation of MMZ is the observed change in the CH_2/CH_3 ratio, which increases with time of exposure of the zeolite to DMM. This is exactly what would be expected from Fig. 3.

Comparison of the bands for DMM chemisorbed on FAU and physisorbed on SiO_2 (Table 1) shows the appearance of several new features, some of which were also observed when both chemisorbed and physisorbed species were present during DMM flow. These new bands occur at 2995, 2982, 2802, 1734, 1490, 1458, 1435, 1417, and 1385 cm^{-1} and may be associated with surface species other than MMZ generated by the disproportionation of DMM (see below). However, all of these new bands were small peaks or shoulders on the bands associated with MMZ, indicating that MMZ was the principal adsorbed species.

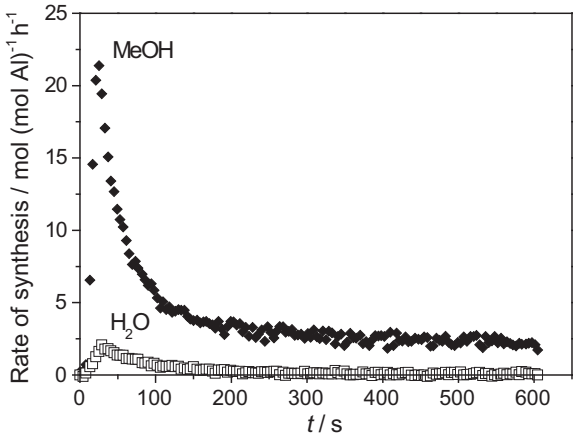

Fig. 4. Rates of methanol and H_2O synthesis over H-FAU at very short times after initial exposure to 0.017 atm DMM/He. 0.03 g catalyst, 383 K, 100 cm^3 min^{-1} at 1 atm.

3.2. FTIR spectra of DME, MF, MMAc, and their derivatives

Table 2 lists the IR bands observed when 0.01 atm DME in He (total flow rate = 100 cm^3 min^{-1}) was passed over SiO_2 and FAU. Also listed in Table 2 are the bands observed after the removal of physisorbed DME from FAU by flushing the infrared cell with He. The assignment of these bands to specific vibrational modes is based on gas-phase DME [24] and DME adsorbed on MFI [25]. Similar results are presented in Table 3 for MF, and here too the band assignments are based on the results of previous studies [26,27]. Table 4 lists the bands reported in the literature for liquid-phase MMAc [28]. Assignments of these bands were made by analogy with DMM, as it has been shown that spectra of species containing CH_3OCH_2 groups, such as DMM and MMAc, tend to show similar C—H stretching and deformation region vibrations [29].

Methoxy species formed by the reaction of DME or methanol with Brønsted acid centers exhibit bands at 2985 and 2885 cm^{-1} [25,30,31]. The absence of such peaks in the spectra for chemisorbed DME on FAU indicates that methoxy species were not formed at 383 K upon exposure of this zeolite to DME. This finding

Table 2
Comparison of vibrational frequencies in DME and DME-like species at 383 K (cm^{-1}).

DME vapor	DME/SiO_2 flowing 0.01 atm DME in He	DME/FAU flowing 0.01 atm DME in He	DME/FAU flowing He	Band assignments
2997 m	2999 m	2998* w	3002* w	a-ν CH_3[a,b]
2937* w	2941 s	2947 s	2967 s	a-ν CH_3[a,b]
	2898 w	2907* w	2914 w	a-ν CH_3[b]
2878* w	2879 w	2877* w		Combination[b]
		2856* w	2858 m	s-ν CH_3[b]
2815 s	2831 s	2833 m	2843 w	s-ν CH_3[a,b]
		2804* w	2806 w	
1462 w	1476 w			δ CH_3[a,b]
1453 s	1459 s	1459 s		δ CH_3[a,b]
		1448 w	1448 s	
		1417 w	1416 w	
			1390 m	
		1384 w	1384 m	

* Frequency estimated from a peak shoulder.
[a] Band assignments based on DME vapor [24].
[b] Band assignments based DME adsorbed on MFI [25].

Table 3
Comparison of vibrational frequencies in MF and MF-like species at 383 K (cm^{-1}).

MF vapor	MF/SiO_2 flowing 0.01 atm MF in He	MF/FAU flowing 0.01 atm MF in He	MF/FAU flowing He	Band assignments
3041 m	3043 m	3045* w		a-ν CH_3[a,b]
3007 m	3011 m	3020* w	3010* w	a-ν CH_3[a,b]
		2980* w	2980 m	
2965 s	2963 s	2965 s	2960 s	s-ν CH_3[a,b]
2939 s	2949 m	2945* w	2945* w	s-ν CH[a,b]
	2900* w	2895* w		Unassigned[b]
2847 w	2862 m	2856 m	2857 s	Unassigned[b]
	2790* w			
1754 s				ν C=O[a]
		1734* w	1734 m	ν C=O[c]
	1722 s	1722* s		ν C=O[b]
1464 m	1465* w		1472* w	a-δ CH_3[a]
1452 s	1453 s	1456 m	1459 m	a-δ CH_3[a,b]
1437 m	1437 s	1436 s	1438 m	s-δ CH_3[a,b]
		1416 w	1415 w	
	1406 w	1406 w	1406 m	
		1395 w	1396 m	
		1390 w	1390 w	
1371 w	1380 m	1379 m	1382 w	δ CH[a,b]

* Frequency estimated from a peak shoulder.
[a] Band assignments based on MF vapor [26].
[b] Band assignments based on MF physisorbed on SiO_2 [27].
[c] Band assignment for surface formates from this work.

Table 4
Vibrational frequencies in liquid MMAc [28] (cm^{-1}).

MMAc liquid	Band assignments[a]
2996 m	a-ν CH_3
2956 s	a-ν CH_2
2932* w	s-ν CH_3
2904* m	s-ν CH_2
2831 m	s-ν CH_3
1761 s	ν C=O
1742* w	
1468* w	s-δ CH_3
1442 s	a-δ CH_3
1381 m	δ CH_2 wagging

* Frequency estimated from a peak shoulder.
[a] Band assignments based on assignments for similar groups in DMM [19].

is consistent with the observation that surface methoxy species are generated from hydrogen-bonded DME at temperatures closer to 473 K [25]. The generation of surface methoxy species at lower temperatures is highly disfavored because of the relatively high activation energy associated with their formation [32].

3.3. Mechanisms of DMM carbonylation and disproportionation

Fig. 5 shows the proposed catalytic cycles for DMM carbonylation (Reactions 2/2′ and 3/3′) and DMM disproportionation (Reactions 4–6). This scheme is adapted from [14] to incorporate new evidence presented here. DMM carbonylation takes place in two steps. In the first step, Reaction 2, CO reacts with methoxymethoxy species (MMZ) to form a methoxyacetyl species (MAZ). MAZ then undergoes methoxylation by DMM, Reaction 3, to release MMAc and regenerate MMZ. Reactions 2 and 3 are both reversible as suggested by the observation that at higher temperatures, the rate of MMAc formation decreases [14]. In the first step of DMM disproportionation, MMZ reacts with another molecule of DMM resulting in hydrogen transfer to form a dimethoxymethoxy species (DMZ) and DME (Reaction 4). DMZ then decomposes to release a second molecule of DME and form a formate species (MFZ), Reaction 5, which then undergoes methoxylation by DMM to release MF and regenerate MMZ, Reaction 6. In what follows, we present evidence to support the proposed schemes for MMAc formation and DMM disproportionation. The kinetics of these processes are discussed in Section 3.6.

Both under DMM flow (Fig. 1) and after flushing with He (Fig. 2), a small peak at 1734 cm^{-1} was observed superimposed over a broader band located between ~1700 and ~1800 cm^{-1}, which grew in the presence of DMM vapor (Fig. 1). The peak at 1734 cm^{-1} is similar to that observed when MF was sorbed on FAU (Table 3), and therefore, this band is assigned to a C=O stretching mode in chemisorbed MF.

Surface formate species in zeolites can be either mono- or bidentate coordinated [33]. Monodentate surface formates exhibit a peak for C=O stretching above 1700 cm^{-1} and a peak for C—O stretching below 1350 cm^{-1}, whereas bidentate formates exhibit asymmetric and symmetric O=C—O stretching vibrations around 1610 cm^{-1} and 1385 cm^{-1} [34]. Similar peaks have been reported for MF adsorbed on alumina [35]. The presence of bands near 1385 cm^{-1} for both DMM and MF chemisorbed on FAU (Tables 1 and 3) could indicate the formation of bidentate formates, whereas the peak at 1734 cm^{-1} could be assigned to C=O stretching vibrations of monodentate formates (MFZ in Fig. 5). In summary, the presence of the peak at 1734 cm^{-1} in Fig. 1 indicates the formation of products of DMM disproportionation.

The band between ~1700 and ~1800 cm^{-1} is associated with the interaction of strongly adsorbed species with the zeolite framework [36]. This feature was observed whenever DMM, DME, or MF were present in the gas phase and diminished in intensity when these gases were flushed from the IR cell with either He or CO.

In addition to the peaks at 1734 cm^{-1} and 1385 cm^{-1}, peaks were observed at 2982, 1458, and 1417 cm^{-1} in the spectra obtained when DMM was contacted with FAU (Figs. 1 and 2), but not SiO_2 (Table 1). These features could also be seen upon exposure of FAU to MF (Tables 2), supporting the assignment of these bands to intermediates involved in the disproportionation of DMM.

Further evidence supporting the relationship between the peak at 1734 cm^{-1} and the production of MF was obtained by collecting a series of spectra in "batch mode" (Fig. 6). After exposing FAU to 0.01 atm DMM in He flowing at 100 cm^3 min^{-1} (Fig. 6, black), the inlet and outlet valves of the IR cell were closed, sealing a small volume of the reactant gas in the cell. The IR cell then acted as a batch reactor. Under these conditions, the band at 1734 cm^{-1} grew initially, reached a maximum intensity after 5188 s and then began to decline. This band was accompanied by a peak at 1722 cm^{-1}, which grew and then decayed somewhat more slowly than the

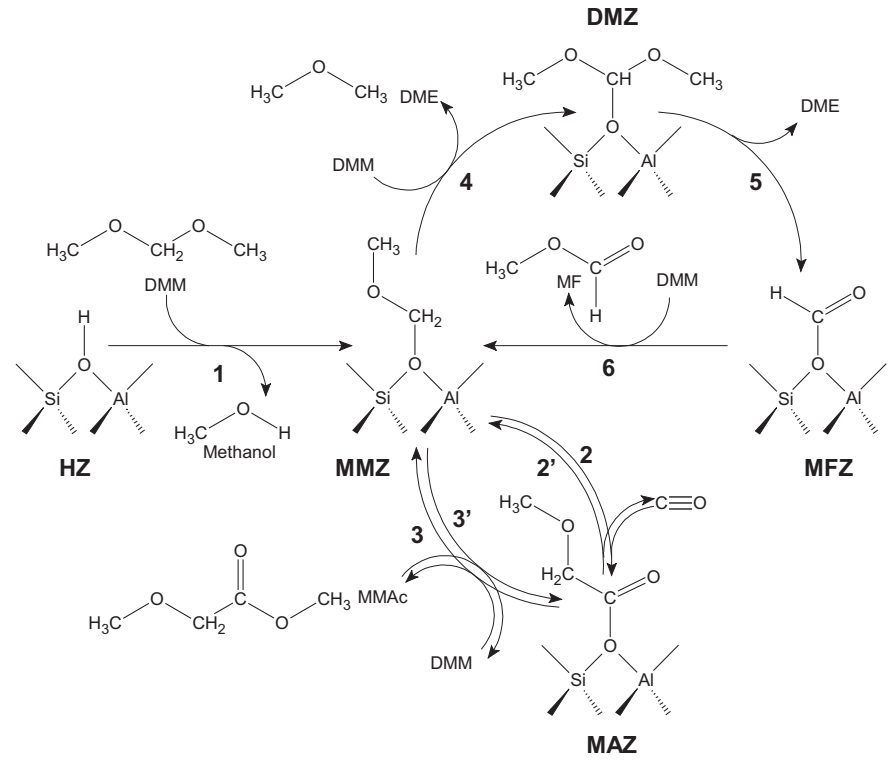

Fig. 5. Proposed reaction mechanism for DMM adsorption (1), DMM carbonylation (2–3), and DMM disproportionation (4–6).

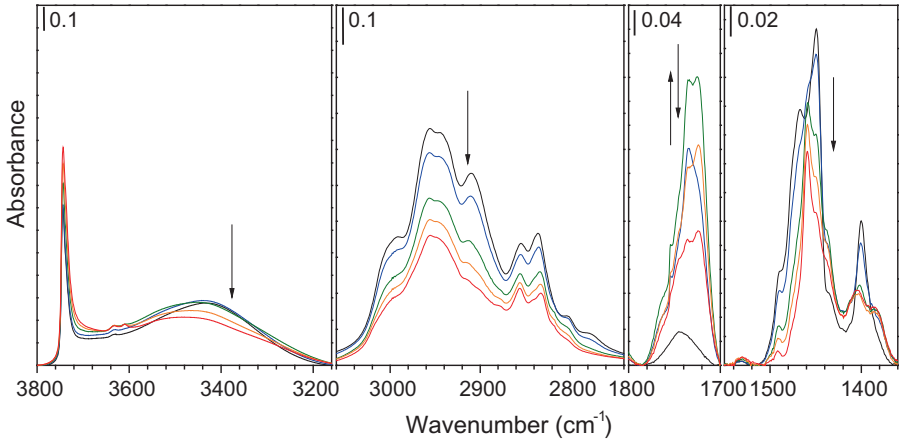

Fig. 6. IR spectra recorded during transient-response experiments of FAU under a stagnant atmosphere initially composed of 0.01 atm DMM/He. Black 0 s, blue 857 s, green 5188 s, orange 11,181 s, red 21,968 s. 0.0479 g catalyst, 383 K, initially at 1 atm.

peak at 1734 cm^{-1}. The band at 1722 cm^{-1} can be assigned to physisorbed MF, as observed on SiO_2 (Table 3, [27,29]), suggesting that MFZ is the precursor to physisorbed MF. The concentration of physisorbed MF was sufficiently large to form some gas-phase MF as evidenced by the presence of the Q branch observed at 1754 cm^{-1} and the R branch at 1768 cm^{-1} [26,27]. The P branch was obscured by the peaks for MFZ and physisorbed MF. The C—H deformation region of the spectrum taken at the end of the batch mode experiment showed several bands and intensities in common with those generated by adsorbing MF on FAU.

DMZ is proposed as an intermediate in the disproportionation of DMM. As noted in Fig. 5, it is thought that DMZ is formed by the reaction of MMZ with DMM and then to decompose to form MFZ. The structure proposed for DMZ was chosen to satisfy both the stoichiometry of the overall disproportionation reaction and the product of a hydrogen-transfer reaction (Reaction 4) between DMM and MMZ. The presence of DMZ may help account for some of the CH_3 deformation vibrations seen in DMM chemisorbed on FAU (e.g., Fig. 1) as some of these bands coincide with vibrations of trimethyl orthoformate, which possesses a structure very similar to DMZ [37].

Fig. 7 shows a series of spectra taken after exposing a FAU surface with previously chemisorbed DMM to pure CO flowing at 100 $cm^3\ min^{-1}$. While little change occurred in the O—H and C—H stretching vibration regions, three new bands appeared in the C=O stretching region. The peak at 1734 cm^{-1} became a shoulder on a new peak that appeared at 1744 cm^{-1} together with two smaller peaks at 1765 and 1718 cm^{-1}. The largest of these new

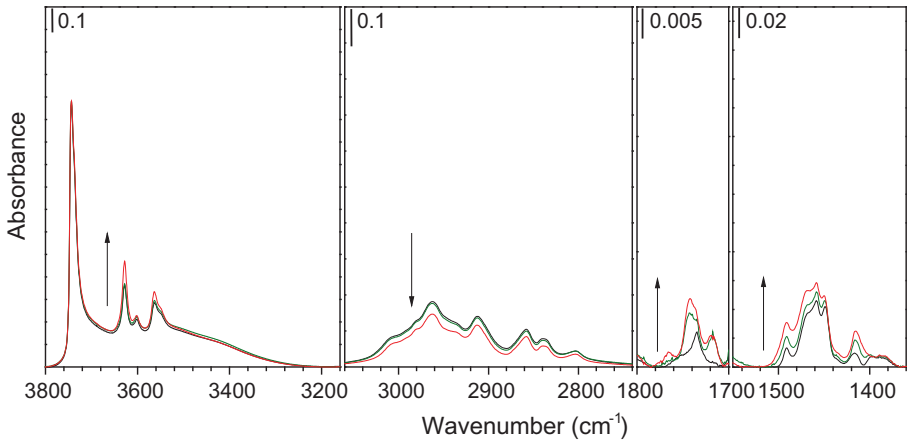

Fig. 7. IR spectra recorded during transient-response experiments of FAU under 1 atm CO following He flush after exposure to 0.01 atm DMM/He. Black 0 s, blue 271 s, green 1398 s, red 5476 s. 0.0479 g catalyst, 383 K, 100 cm^3 min^{-1} at 1 atm.

peaks, the one at 1744 cm^{-1}, is attributed to the C=O stretching vibration of MAZ. As shown in Fig. 5, this species is formed by carbonylation of MMZ.

After flushing CO from the IR cell with He, the catalyst was again exposed to 0.01 atm DMM in He flowing at 100 cm^3 min^{-1}. The spectrum recorded at this point is shown in black in Fig. 8. The feed to the IR cell was then switched to 0.01 atm DMM in CO flowing at 100 cm^3 min^{-1}. The resulting spectra are shown in Fig. 8. The C=O stretching vibration of MAZ at 1744 cm^{-1} rapidly grew in intensity in the presence of both CO and DMM in the gas phase, and the maximum intensity reached was far greater than that attained in the presence of CO alone. Very little change was observed in the rest of the spectrum, consistent with the fact that both MMZ and MAZ possess the same ratio of CH_2 to CH_3 groups (see Reaction 2 in Fig. 5).

Comparison of the spectra presented in Figs. 7 and 8 shows that when CO alone was passed over FAU containing MMZ (Fig. 7), the extent of CO insertion into the framework O—C bond of MMZ to form MAZ was far less than when the same surface was exposed to CO and DMM simultaneously (Fig. 8). This is clearly evidenced by the changes in intensity of the peak at 1744 cm^{-1} in the two cases. The peak intensity in the presence of DMM was ~4.5 times greater than that reached without DMM, suggesting that the presence of DMM enhances the rate of CO insertion. As discussed below, this is thought to be due to stabilization of the carbocationic transition state involved in the carbonylation of MMZ (Reaction 2 in Fig. 5). To support this hypothesis, FAU was exposed to DMM and then flushed with He to generate MMZ species without physisorbed DMM, as in Fig. 2. The zeolite was then exposed to CO as in Fig. 8, generating a small peak for the C=O stretch of MAZ at 1744 cm^{-1}. The gas flow was then switched to 0.01 atm DME in CO. The C=O stretch of MAZ increased by a factor of ~4.5 when DME was present in the gas phase relative to when the gas phase was pure CO. Thus, both DME and DMM were found to increase the intensity of the C=O stretching band of MAZ by a similar factor of ~4.5 relative to what was observed in the absence of either gas. This effect is thought to be due to solvation of the carbocationic transition state involved in Reaction 2 by nucleophilic oxygen atoms in DMM and DME, in a manner similar to what is known to occur in liquid-phase systems [38–40].

Upon reaching steady state under flow of CO and DMM (Fig. 8, red curve), the rates of DME, MF, and MMAc formation from the catalyst in the IR cell were comparable to the rates previously reported under similar conditions [14].

The effect of CO pressure on the carbonylation of MMZ to form MAZ is shown in Fig. 9. Increasing the CO pressure from 0 to 3 atm had almost no effect on the C—H stretching and deformation regions of the spectra but increased the intensity of the C=O stretching frequency of MAZ at 1744 cm^{-1}. The intensities of the C—H vibrations should not change very much because both MMZ and

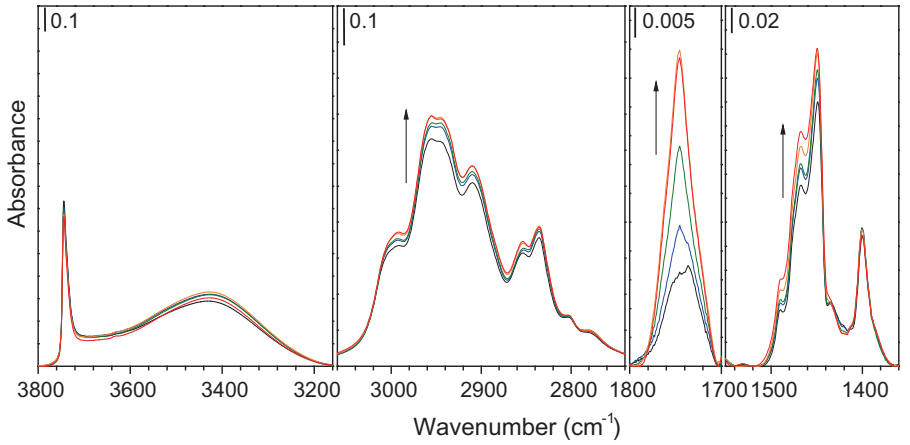

Fig. 8. IR spectra recorded during transient-response experiments of FAU under 0.01 atm DMM/CO following exposure to 0.01 atm DMM/He. Black 0 s, blue 182 s, green 547 s, orange 4463 s, red 7764 s. 0.0479 g catalyst, 383 K, 100 cm^3 min^{-1} at 1 atm.

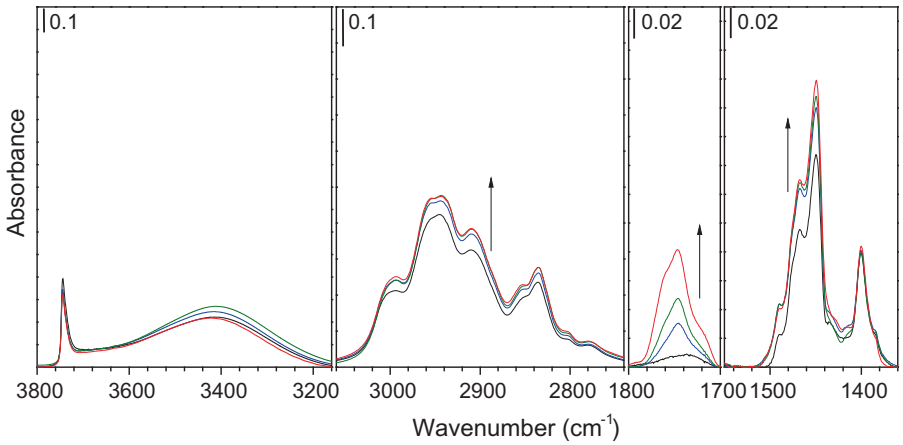

Fig. 9. Spectra of FAU under 0.01 atm of DMM and different CO partial pressures. Black P_{CO} = 0 atm (balance He), blue P_{CO} = 1.0 atm, green P_{CO} = 2.0 atm, P_{CO} = 3.0 atm. 0.0272 g catalyst, 383 K, 100 cm^3 min^{-1} at reaction pressure, 100–300 cm^3 min^{-1} at STP.

MAZ contain CH_3OCH_2 groups and hence would be expected to exhibit similar spectra in the C—H stretching and deformation regions [29]. Moreover, if the extent of conversion of MMZ to MAZ via CO insertion was small, any changes in the appearance of the spectrum in the C—H stretching regime would be difficult to detect. The apparent peaks appearing on either side of the band at 1744 cm^{-1} seen at higher pressures result from an interference pattern created by multiple reflections of the IR beam in the gaps between the CaF_2 windows contained in the IR cell.

The intensity of the C=O stretching vibration of MAZ, measured as the peak height normalized by the pellet weight, can be compared to the rate of MMAc formation at steady state. Fig. 10 shows that both increased nearly linearly with CO pressure from 0 atm up to 3 atm. Since peak intensities of absorbance spectra follow the Beer–Lambert law, the intensity of the C=O stretching vibration of MAZ is directly proportional to the concentration of MAZ on the surface of FAU. Because both the IR peak intensities and steady-state MMAc synthesis rates showed the same linear dependence on the CO pressure, the rate of MMAc formation must therefore be proportional to the concentration of MAZ, as suggested by Reaction 3 in Fig. 5.

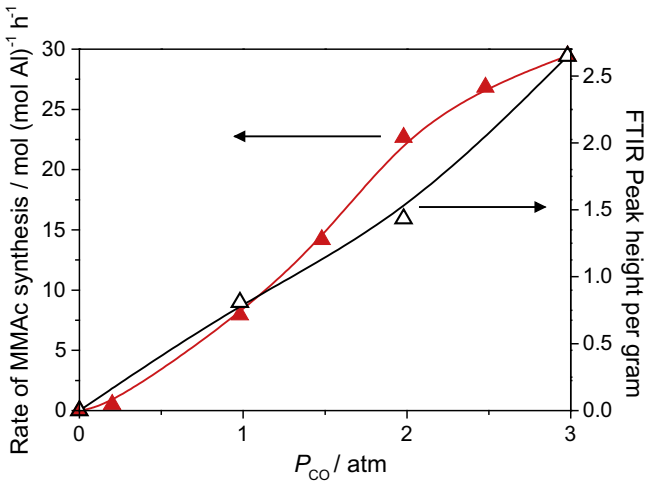

Fig. 10. Comparison of the effect of CO partial pressure on steady-state MMAc formation rate over FAU (left axis) and normalized peak height of peak at 1744 cm^{-1} (right axis). Steady-state data, 0.05 g catalyst, 383 K, P_{DMM} = 0.013–0.019 atm, 100 cm^3 min^{-1} at reaction pressure, 100–300 cm^3 min^{-1} at STP. FTIR peak height, 0.0272 g catalyst, 383 K, P_{DMM} = 0.01 atm, 100 cm^3 min^{-1} at reaction pressure, 100–300 cm^3 min^{-1} at STP.

3.4. DMM carbonylation and disproportionation over MFI

The spectrum of H-MFI (Si/Al ≈ 27.5) is shown in Fig. 11 (black). The large peak at 3610 cm^{-1} is assigned to the Brønsted acid site of MFI, and the smaller peaks at 3743 and 3722 cm^{-1} are assigned to external and internal silanol groups, respectively [30]. Because MFI can be synthesized directly in high Si/Al ratios, the number of SiOH defect sites is small compared to that in FAU. A shoulder around 3660 cm^{-1} is likely assigned to extra-framework alumina (EFAL) species [30,31]. The small size of this peak indicates that EFAL species were present in small concentrations.

MFI was exposed to 0.01 atm DMM in He flowing at 100 cm^3 min^{-1}. The resulting spectrum is shown in Fig. 11 (blue). The Brønsted acid peak disappeared upon interaction of DMM with the zeolite. No peak for physisorbed DMM was observed in the O—H stretching region, when compared to the broad peak at 3430 cm^{-1} observed on FAU because of the far smaller concentration of SiOH groups on which to adsorb. The C—H stretching and C—H deformation regions are very similar to those observed when FAU is contacted with DMM, indicating that the species formed in MFI are similar to those formed in FAU, either MMZ or DMM physisorbed on Brønsted acid sites. By contrast, though, the deformations bands at 1457, 1436, and 1381 cm^{-1} were more prominent for MFI than for FAU. These bands were tentatively assigned to surface intermediates associated with the disproportionation of DMM and were prominent in the spectra recorded upon exposing FAU to MF as well (Table 3). The peak at 1734 cm^{-1} was much more intense than the same band assigned to MFZ on FAU, indicating a greater rate of DMM disproportionation over MFI compared to FAU [14].

Upon flushing the IR cell with He, physisorbed and vapor-phase species were removed, leaving behind only chemisorbed species (Fig. 11, red). In contrast to FAU, the spectrum generated in this manner over MFI differed significantly from the spectrum of gaseous DMM and DMM physisorbed on SiO_2, indicating that a DMM-like molecule was either absent or did not constitute the majority species. The most significant change was in the C—H deformation region, where peaks at 1456, 1437, and 1381 cm^{-1}, and peak shoulders at 1409 cm^{-1}, 1400 cm^{-1}, and 1388 cm^{-1} were observed, while peaks at 1475, 1467, and 1450 cm^{-1}, characteristic of DMM-like molecules (Table 1), were absent. The observed C—H deformation vibrations were similar to the spectrum of MF chemisorbed on FAU (Table 3), suggesting that the adsorbed species were predominantly disproportionation products. However, the intensity of the C=O stretching mode of MFZ at 1734 cm^{-1} decreased rapidly and did not persist as it did on FAU. Some of the

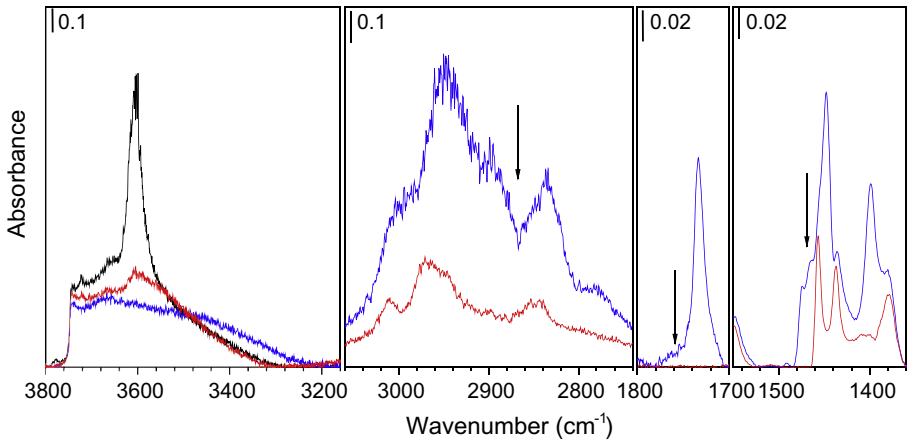

Fig. 11. Spectra of H-MFI under He (black), after 990 s of exposure to 0.01 atm DMM/He (blue), and under He flow for 3214 s after exposure to DMM/He (red). 0.0510 g catalyst, 383 K, 100 cm^3 min^{-1} at 1 atm.

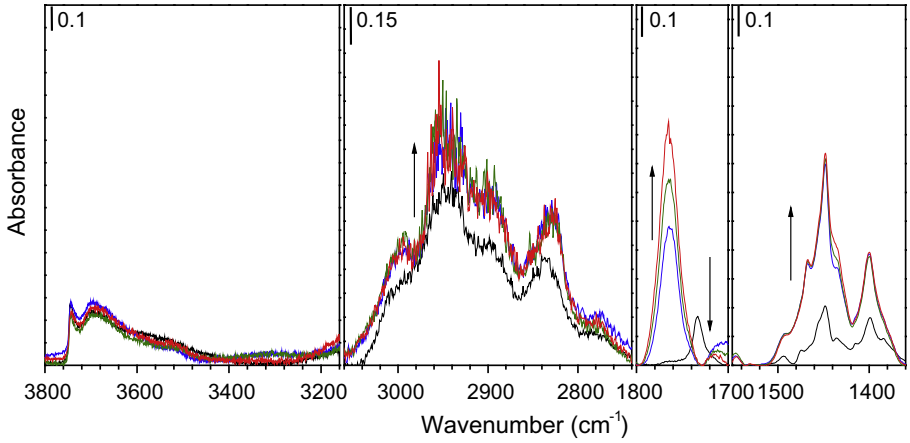

Fig. 12. Spectra of MFI under 0.01 atm of DMM and different CO partial pressures. Black P_{CO} = 0 atm (balance He), blue P_{CO} = 1.0 atm, green P_{CO} = 2.0 atm, P_{CO} = 3.0 atm. 0.0442 g catalyst, 383 K, 100 cm^3 min^{-1} at reaction pressure, 100–300 cm^3 min^{-1} at STP.

C—H stretching vibration frequencies observed, 3009, 2970, 2949, 2854, and 2843 cm^{-1}, were similar to bands found in the spectra of MF and DMM chemisorbed on FAU.

After flushing the IR cell with He as described above, a flow of 100 cm^3 min^{-1} CO was introduced. In contrast to what was observed for FAU, no evidence was seen for carbonylation. However, exposing MFI to CO in this manner did have an irreversible effect on the DMM disproportionation activity. When the gas flow was switched to 100 cm^3 min^{-1} of 0.01 atm of DMM in He, a smaller peak at 1734 cm^{-1} for MFZ was formed compared to that observed before the introduction of CO. This poisoning of disproportionation activity by CO was also observed for MFI in steady-state kinetic experiments, but not for FAU [14], and introduction of CO had little lasting effect on the surface species on FAU as observed by FTIR spectroscopy.

The inhibition of DMM disproportionation over MFI was also observed under reaction conditions when the gas flow was switched from 100 cm^3 min^{-1} of 0.01 atm DMM in He (Fig. 12 black) to 100 cm^3 min^{-1} of 0.01 atm DMM in CO (Fig. 12 blue). The MFZ peak at 1734 cm^{-1} disappeared, and the C—H deformation region of the spectrum became similar to that generated under similar conditions on FAU. This indicates that the more species containing CH_3OCH_2 groups, such as MMZ and MAZ, and fewer species associated with disproportionation, such as MFZ, were adsorbed in MFI. At the same time, the C=O stretch of MAZ appeared at 1763 cm^{-1}. Increasing the CO pressure to 2 atm (Fig. 12 green) and 3 atm (Fig. 12 red) caused little change in the rest of the spectrum aside from the increase in the intensity of the C=O stretching band of MAZ.

Fig. 13 compares the steady-state rate of MMAc formation with the intensity of the C=O stretching vibration at 1763 cm^{-1} for MAZ. As with FAU, the steady-state kinetic data and the IR peak intensities showed similar trends with increasing CO partial pressure. Unlike FAU, both increased with less than first-order dependence on the CO pressure. Although the rate of MMAc synthesis was ~5× greater on FAU than on MFI, the intensity of the peak for C=O stretching vibrations of MAZ normalized by the catalyst pellet mass was ~10× larger for MFI than for FAU. This indicates that the concentration of MAZ species was higher for MFI than for FAU, and suggests that the rate of removal of MAZ to form MMAc is much higher on FAU than on MFI. This conclusion is supported by analysis of the energetics of DMM carbonylation [15].

The relative concentrations of MAZ observed by IR spectroscopy on FAU and MFI can be rationalized in terms of recent theoretical calculations carried out at the DFT/B3LYP/6-311++G(3df, 3pd) level [15]. Fig. 14 shows the potential energy profile as a function of reaction coordinate for FAU and MFI. The zero on the potential energy diagram is for MMZ and gas-phase CO. MMAc is formed in two steps – carbonylation of MMZ followed by a methoxylation of the resulting MAZ. The calculated barrier for MMZ carbonylation

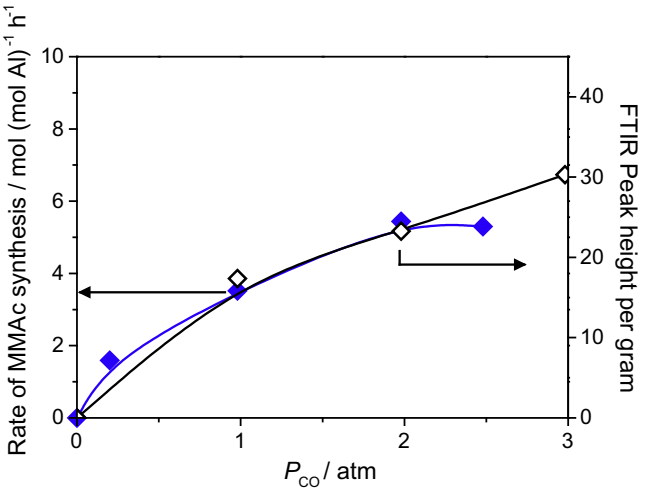

Fig. 13. Comparison of the effect of CO partial pressure on steady-state MMAc formation rate over MFI (left axis) and normalized peak height of peak at 1763 cm^{-1} (right axis). Steady-state data, 0.05 g catalyst, 383 K, P_{DMM} = 0.013–0.019 atm, 100 cm^3 min^{-1} at reaction pressure, 100–300 cm^3 min^{-1} at STP. FTIR peak height, 0.0442 g catalyst, 383 K, P_{DMM} = 0.01 atm, 100 cm^3 min^{-1} at reaction pressure, 100–300 cm^3 min^{-1} at STP.

is 58 kJ/mol for MFI and 74 kJ/mol for FAU, whereas the calculated activation barrier for methoxylation of MAZ is 63 kJ/mol for MFI and 32 kJ/mol for FAU. The smaller activation barrier for methoxylation of MAZ on FAU relative to MFI means that MAZ would be expected to react with DMM more readily on FAU than MFI. Because of the larger methoxylation barrier over MFI, MAZ accumulates on this zeolite more than on FAU, leading to the expectation of a higher surface concentration of MAZ on MFI than FAU, consistent with what is observed (see Figs. 10 and 13).

3.5. Derivation of the kinetic rate expression and the plug-flow reactor model

The kinetics of DMM disproportionation and carbonylation can be developed from the mechanism presented in Fig. 5. Since Reaction 1 only occurs for a short time immediately after exposing the catalyst to DMM, it does not affect the steady-state kinetics. In the expressions below, r_i is the rate of formation of gaseous species i, k_j is the rate constant for reaction j, P_k is the partial pressure of gaseous species k, θ_l is the surface coverage of surface species l. By treating each of Reactions 2–6 as elementary, the rates of MMAc, DME, and MF formation can be expressed as:

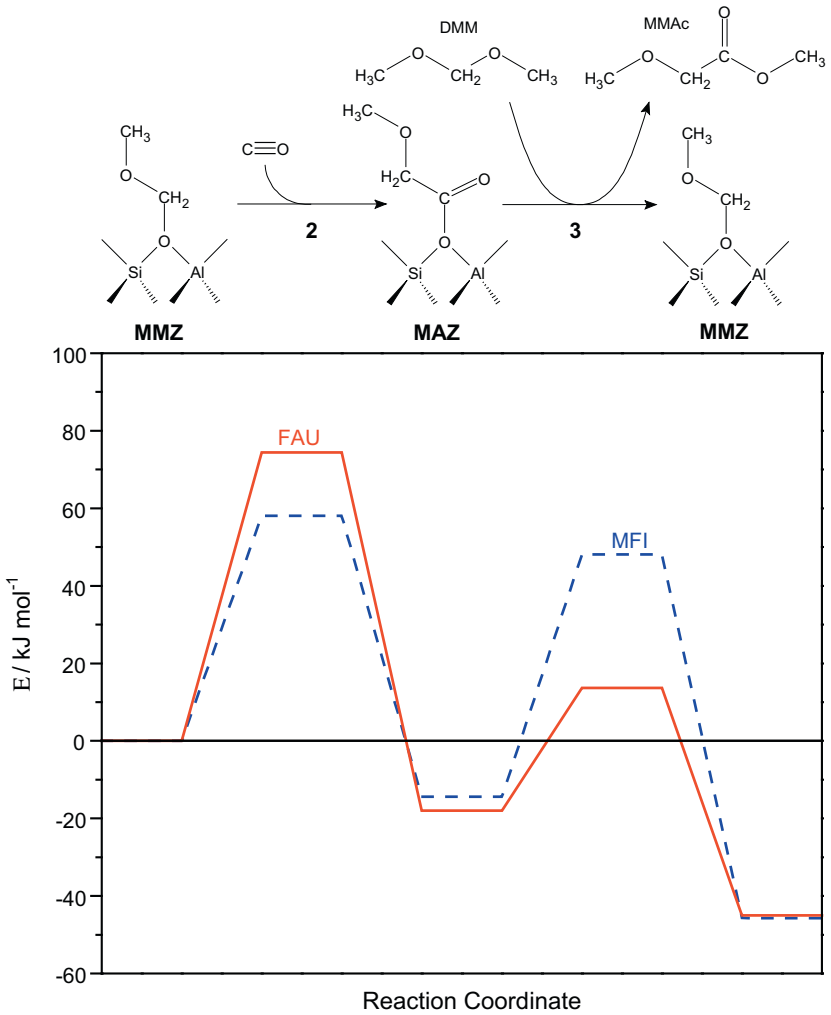

Fig. 14. Theoretically projected energy profile for MMAc formation calculated at the B3LYP/6-311++G(3df, 3pd) level of theory with zero-point energy calculated at the B3LYP/6-31G* level of theory [15]. Calculations performed on 36 T atom cluster for FAU and 44 T atom cluster.

$$r_{MMAc} = k_3 P_{DMM}\theta_{MAZ} - k_{3'} P_{MMAc}\theta_{MMZ}$$
$$r_{DME} = k_4 P_{DMM}\theta_{MMZ} + k_5\theta_{DMZ}$$
$$r_{MF} = k_6 P_{DMM}\theta_{MFZ}$$

The rate of accumulation of each surface species (MMZ, MAZ, DMZ, and MFZ) can be written as:

$$\frac{d\theta_{MMZ}}{dt} = -k_2 P_{CO}\theta_{MMZ} + k_{2'}\theta_{MAZ} + k_3 P_{DMM}\theta_{MAZ} - k_{3'} P_{MMAc}\theta_{MMZ} - k_4 P_{DMM}\theta_{MMZ} + k_6 P_{DMM}\theta_{MFZ}\frac{d\theta_{MAZ}}{dt}$$
$$= k_2 P_{CO}\theta_{MMZ} - k_{2'}\theta_{MAZ} - k_3 P_{DMM}\theta_{MAZ} + k_{3'} P_{MMAc}\theta_{MMZ}\frac{d\theta_{DMZ}}{dt}$$
$$= k_4 P_{DMM}\theta_{MMZ} - k_5\theta_{DMZ}\frac{d\theta_{MFZ}}{dt} = k_5\theta_{DMZ} - k_6 P_{DMM}\theta_{MFZ}$$

Applying the pseudo-steady-state hypothesis to each surface species and setting each of the above expressions to zero results in the following expressions for the surface coverages, θ_l:

$$\theta_{MAZ} = \frac{k_2 P_{CO} + k_{3'} P_{MMAc}}{k_{2'} + k_3 P_{DMM}}\theta_{MMZ}$$
$$\theta_{DMZ} = \frac{k_4}{k_5} P_{DMM}\theta_{MMZ}$$
$$\theta_{MFZ} = \frac{k_4}{k_6}\theta_{MMZ}$$

By combining the above equations, the rates of formation of the products can be written as:

$$r_{MMAc} = \frac{k_2 P_{CO} k_3 P_{DMM} - k_{2'} k_{3'} P_{MMAc}}{k_{2'} + k_3 P_{DMM}}\theta_{MMZ} \quad (1)$$
$$r_{DME} = 2k_4 P_{DMM}\theta_{MMZ} = 2r_{MF}$$
$$r_{DMM} = -r_{MMAc} - r_{DME}$$

Applying a site balance to surface species MMZ, MAZ, DMZ, and MFZ gives the following expression for θ_{MMZ}:

$$\theta_{MMZ} = \left(1 + \frac{k_2 P_{CO} + k_{3'} P_{MMAc}}{k_{2'} + k_3 P_{DMM}} + \frac{k_4}{k_5} P_{DMM} + \frac{k_4}{k_6}\right)^{-1} \quad (2)$$

By treating the reactor as an isothermal, plug-flow reactor, the mole balance for any species can be written as a first-order differential equation in species pressure, P_i. Eq. (3) assumes that the change in the total volumetric flow rate is small (due to the large excess of CO used):

$$\frac{dF_i}{dW} = \frac{Q}{RT}\frac{dP_i}{dW} = r_i \quad \text{or} \quad W = \frac{Q}{RT}\int_{P_{i0}}^{P_i}\frac{dP_i}{r_i} \quad (3)$$

Here F_i is the molar flow rate of species i in the gas phase, W is the moles of active sites or Al atoms in the sample, Q is the total gas volumetric flow rate, R is the molar gas constant, T is the reaction temperature, and P_{i0} is the initial partial pressure of species i at the reactor inlet. Substituting for r_{DMM} and assuming that P_{CO} was constant (again due to large excess of CO used), the following expression is obtained:

$$W = -\frac{Q}{RT}\int_{P_{DMM0}}^{P_{DMM}}\frac{(k_{2'} + \frac{k_{2'}k_4}{k_6} + k_2 P_{CO}) + \left(k_3 + \frac{k_{2'}k_4}{k_5} + \frac{k_3 k_4}{k_6}\right)P_{DMM} + \frac{k_3 k_4}{k_5}P_{DMM}^2 + k_{3'} P_{MMAc}}{(k_2 k_3 P_{CO} + 2k_{2'}k_4)P_{DMM} + 2k_3 k_4 P_{DMM}^2 - k_{2'}k_{3'} P_{MMAc}} dP_{DMM} \quad (4)$$

Assuming that $k_{3'}P_{MMAc}$ was small and eliminating this product from Eq. (4), the analytical solution is:

$$W = -\frac{Q}{RT}\left[\frac{\frac{1}{2k_5}(P_{DMM} - P_{DMM,0}) + \frac{k_{2'} + \frac{k_{2'}k_4}{k_6} + k_2 P_{CO}}{k_2 k_3 P_{CO} + 2k_{2'}k_4}\ln\frac{P_{DMM}}{P_{DMM,0}} + \left(\frac{k_2 k_3 P_{CO}}{2k_4} + \frac{k_2 k_3 P_{CO}}{2k_6} - \frac{k_2^2 k_3 P_{CO}^2}{4k_4 k_5} - \frac{k_2 k_{2'} P_{CO}}{2k_5} + \frac{2k_{2'}k_4}{k_6} + k_2 P_{CO}\right)}{(k_2 k_3 P_{CO} + 2k_{2'}k_4)}\ln\frac{(k_2 k_3 P_{CO} + 2k_{2'}k_4 + 2k_3 k_4 P_{DMM})}{(k_2 k_3 P_{CO} + 2k_{2'}k_4 + 2k_3 k_4 P_{DMM,0})}\right] \quad (5)$$

from which P_{DMM} at the reactor exit can be solved for iteratively. By substituting Eqs. (1) and (2) into Eq. (3), P_{MMAc} and P_{DME} can be determined from:

$$\int_0^{P_{MMAc}} dP_{MMAc} = -\int_{P_{DMM0}}^{P_{DMM}}\frac{k_2 P_{CO} k_3}{k_2 P_{CO} k_3 + 2k_{2'}k_4 + 2k_3 k_4 P_{DMM}} dP_{DMM}$$
$$P_{MMAc} = -\frac{k_2 P_{CO}}{2k_4}\ln\frac{(k_2 P_{CO} k_3 + 2k_{2'}k_4 + 2k_3 k_4 P_{DMM})}{(k_2 P_{CO} k_3 + 2k_{2'}k_4 + 2k_3 k_4 P_{DMM,0})} \quad (6)$$

and

$$P_{DME} = P_{DMM,0} - P_{DMM} - P_{MMAc} \quad (7)$$

3.6. Determination of kinetic rate parameters and reactor model results

To evaluate the effectiveness of Eqs. (5)–(7) for describing the kinetics of MMAc, DME, and MF requires estimates for the values of the pre-exponential factor (A) and activation energy (E_a) for each of the rate coefficients appearing in these equations. All pre-exponential factors were constrained to lie within the range of values expected for unimolecular (10^{13}–10^{17} s^{-1}) and bimolecular reactions involving a gas-phase reactant and an adsorbed reactant (10^2–10^{13} atm^{-1} s^{-1}) [41,42]. Estimates for E_a for Reactions 2, 2′, and 3 were obtained by adjusting the values obtained from DFT calculations [15] (see Fig. 14) in order to obtain a good fit to the experimental data for FAU (see Fig. 15a–c below). The values of E_a and A for Reactions 3 and 6 were set equal to each other because of the similarity of the methoxylation reactions. The values of E_a for Reactions 4 and 5 were chosen to be reasonable. Since Reactions 4–6 are irreversible, the fit of theory to experiment was much more sensitive to the value of activation energy chosen for Reaction 4 than Reaction 5.

The value of W in Eq. (5) was taken to be one half of that used experimentally, to account for the observation that only half of the Brønsted acid protons react upon exposure to DMM (see Figs. 4 and 7). The acid sites that did not react with DMM are assumed to be catalytically inactive.

Fig. 15 compares the results of the plug-flow reactor model with the steady-state rates of product formation reported previously as functions of reaction temperature (Fig. 15a), feed CO partial pressure (Fig. 15b), and feed DMM partial pressure (Fig. 15c) [14]. It is evident that the experimentally observed trends in the carbonylation and disproportionation rates for FAU are well described by Eqs. (5)–(7) together with rate parameters listed in Table 5. In particular, the model correctly reproduces the maximum in the rate of MMAc formation and predicts the dependence of the MMAc formation rate on the feed partial pressure of CO and DMM. The model also predicts the correct dependences of the rates of DME and

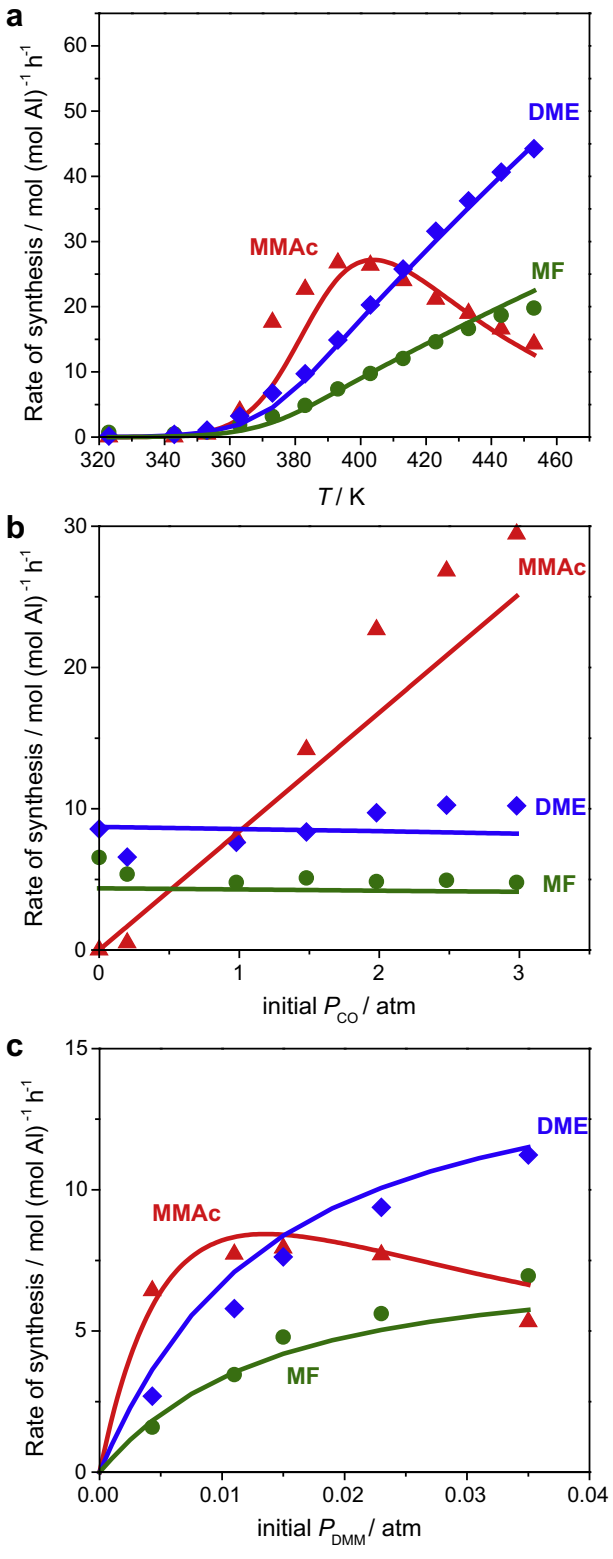

Fig. 15. Comparison of steady-state reaction rate data (symbols) and plug-flow reactor model results (curves) of MMAc, DME, and MF formation rates as a function of (a) reaction temperature, (b) inlet CO partial pressure, and (c) inlet DMM partial pressure. (a) Steady-state data, 0.05 g catalyst, P_{CO} = 1.98 atm, P_{DMM} = 0.017 atm, 100 cm^3 min^{-1} at reaction pressure, 200 cm^3 min^{-1} at STP. Plug-flow reactor model, 0.05 g catalyst, P_{CO} = 1.98 atm, initial P_{DMM} = 0.017 atm, 100 cm^3 min^{-1} at reaction pressure. (b) Steady-state data, 0.05 g catalyst, 383 K, P_{DMM} = 0.013–0.019 atm, 100 cm^3 min^{-1} at reaction pressure, 100–300 cm^3 min^{-1} at STP. Plug-flow reactor model, 0.05 g catalyst, initial P_{DMM} = 0.016 atm, 100 cm^3 min^{-1} at reaction pressure.

Table 5
Activation energies E_a and pre-exponential factors A for FAU (Si/Al ratio ≈30) used in plug-flow reactor model.

Reaction	A[a]	E_a (kJ mol^{-1})	k[a]	$[A] = [k]$
2	1.6×10^6	58	2.0×10^{-2}	atm^{-1} s^{-1}
2′	1.0×10^{17}	108	2.0×10^2	s^{-1}
3	3.1×10^6	17	1.5×10^4	atm^{-1} s^{-1}
3′[b]	[b]	–	–	–
4	3.7×10^2	22	3.7×10^{-1}	atm^{-1} s^{-1}
5	8.0×10^{12}	112	4.3×10^{-3}	s^{-1}
6	3.1×10^6	17	1.5×10^4	atm^{-1} s^{-1}

[a] $k = Ae^{-E_a/RT}$, evaluated at 383 K.
[b] All terms containing $k_{3'}$ were eliminated from Eq. (5), so no values were used in the model.

MF formation as functions of temperature and feed CO and DMM partial pressures.

The following experiment was carried out in order to assess the validity of the choice of rate parameters listed in Table 5. FAU was exposed to 100 cm^3 min^{-1} of 0.01 atm DMM in He. The gas flow was then switched to 100 cm^3 min^{-1} of 0.01 atm DMM in CO, and spectra were recorded every 45 s. The peak height of the C=O stretching vibration of MAZ at 1744 cm^{-1} reached a steady-state value after 1800 s. The gas flow was then switched back to 100 cm^3 min^{-1} of 0.01 atm DMM in He, and spectra were recorded every 45 s. The resulting normalized peak height of the C=O stretching vibration for MAZ is plotted as a function of time in Fig. 16.

The concentration of MAZ on the surface is proportional to the absorbance of the C=O stretching vibration observed. The initial rates of change in the C=O stretching peak following a change in the gas-phase composition are therefore directly proportional to the rate of change in the surface concentration of MAZ, $\frac{d\theta_{MAZ}}{dt}$. The proportionality constant includes the unknown extinction coefficient for the C=O stretching vibration of MAZ, preventing quantitation of the surface coverage directly from the FTIR data. From the proposed mechanism,

$$\frac{d\theta_{MAZ}}{dt} = k_2 P_{CO}\theta_{MMZ} - k_{2'}\theta_{MAZ} - k_3 P_{DMM}\theta_{MAZ} + k_{3'} P_{MMAc}\theta_{MMZ}. \quad (8)$$

The term $k_{3'}P_{MMAc}$ Eq. (8) is small relative to the other terms in the sum and is therefore eliminated. At t = 0 when the gas was initially

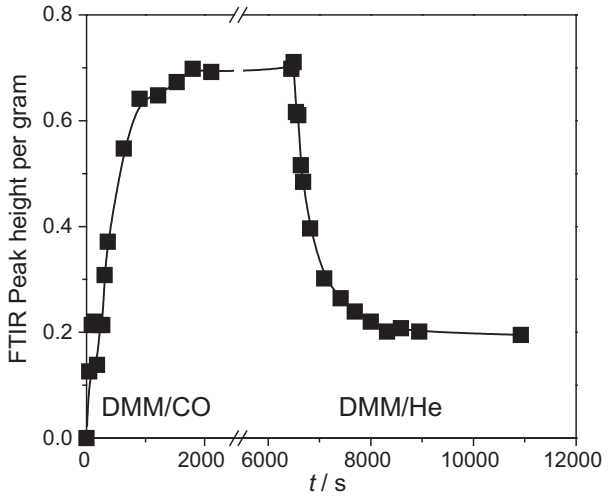

Fig. 16. Growth of MAZ peak as a function of time after switching to DMM/CO flow over FAU saturated with DMM and decline of MAZ peak after switching back to DMM/He. 0.0159 g catalyst, 383 K, 100 cm^3 min^{-1} at 1 atm.

switched from DMM/He to DMM/CO, the surface coverage of MAZ was zero, so the rate of change in the surface coverage of MAZ can be approximated by $\frac{d\theta_{MAZ}}{dt} = k_2 P_{CO}\theta_{MMZ}$. The initial slope at $t = 0$ was measured from Fig. 16 as 1.02×10^{-3} absorbance units $g^{-1}\,s^{-1}$. When the gas flow was switched from DMM/CO back to DMM/He at $t = 6498$ s, the slope of the peak height of the C=O stretch as a function of time was measured as -9.91×10^{-4} absorbance units $g^{-1}\,s^{-1}$. This slope was once again proportional to $\frac{d\theta_{MAZ}}{dt}$. However, this time with no CO in the gas phase and a non-zero MAZ coverage, $\frac{d\theta_{MAZ}}{dt} = -(k_{2'} + k_3 P_{DMM})\theta_{MAZ}$. By taking the ratio of the slopes at $t = 0$ s and $t = 6498$ s obtained from the FTIR measurements, the proportionality constant including the extinction coefficient is eliminated, leading to the expression:

$$\frac{\left.\frac{d\theta_{MAZ}}{dt}\right|_{t=0s}}{\left.\frac{d\theta_{MAZ}}{dt}\right|_{t=6498s}} = -\frac{k_2 P_{CO}\theta_{MMZ}|_{t=0s}}{(k_{2'} + k_3 P_{DMM})\theta_{MAZ}|_{t=6498s}}. \quad (9)$$

The value of the left-hand side of Eq. (9) determined from the experimentally measured slopes is −1.03. The value of the right-hand side of this equation was determined using the plug-flow reactor model to evaluate the average values of θ_{MMZ}, θ_{MAZ}, and P_{DMM}. Using these average values together with the rate constants in Table 5, the value of the right-hand side of Eq. (9) is −0.97, which is in excellent agreement with the experimentally determined value of −1.03. The agreement between experimental kinetic measurements and the plug-flow reactor model indicates that the parameters chosen are reasonable.

A question then remains concerning the differences between the activation energies for Reactions 2, 2′, and 3 determined theoretically (see Fig. 14 and Ref. [15]) and those determined by fitting the observed rates of product formation on FAU as a function of temperature. The values of E_a determined for Reactions 2, 2′, and 3 by DFT calculations are 74, 92, and 32 kJ/mol, respectively, whereas the corresponding values reported in Table 5 obtained from the fit of the rate data shown in Fig. 15a are 58, 108, and 17 kJ/mol, respectively. A part of the difference between theory and experiment could be due to the neglect of dispersion forces in the theoretical calculations. Recent investigations into reactions occurring in zeolites have shown that when such forces are taken into account, the activation barriers for elementary processes can altered by as much as ±10–30 kJ/mol [43–47]. Nevertheless, both sets of activation energies suggest that the formation of MMAc is rate-limited by the carbonylation of MMZ.

4. Conclusions

In situ IR spectra taken during the exposure of FAU and MFI to DMM or DMM and CO show evidence for methoxymethoxy (MMZ), formate (MFZ) and methoxyacetyl (MAZ) groups, species that are proposed as intermediates in the carbonylation and disproportionation of DMM. The response of these species to changes in gas composition is consistent with that anticipated on the basis of steady-state rate data. For example, the intensity of the carbonyl stretch for MAZ, the precursor to MMAc, and the rate of MMAc formation increase in parallel with increasing CO partial pressure for both FAU and MFI. Likewise, the intensity of the MAZ peak observed for MFI is considerably greater than that for FAU, consistent with the lower activity of MFI for MMAc formation. This suggests that the rate of methoxylation of MAZ on MFI is slower than on FAU, consistent with the results of recent DFT calculations. IR observations also reveal that the rate of DMM carbonylation on both FAU and MFI is more rapid in the presence of physisorbed DMM or DME. This effect is attributable to the enhanced stabilization of the carbocationic transition state due to solvation by the physisorbed species. It is also found that the concentration of MFZ, the final precursor to MF, decreases with increasing CO partial pressure for MFI but not for FAU, consistent with the observed effects of CO partial pressure on the rates of DMM disproportionation on both zeolites. Rate expressions for the formation of all reaction products, derived on the basis of the proposed mechanism of DMM carbonylation and disproportionation, give an accurate description of the dependences of the experimentally observed rates on temperature and the feed partial pressures of CO and DMM.

Acknowledgments

The authors would like to acknowledge the contributions of Dr. Vladimir Shapovalov in carrying out DFT calculations to investigate the carbonylation mechanism and estimate the activation energies of the reaction steps, and William C. Vining in preparing a SiO_2 sample for the physisorption of reaction gases. This work was supported by the Methane Conversion Cooperative funded by BP.

References

[1] J.M. Berty, Ethylene oxide synthesis, in: B.L. Leach (Ed.), Applied Industrial Catalysis, vol. 1, Academic Press, New York, 1983, p. 207.
[2] R.L. Pruett, W.E. Walker, U.S. Patent 3 957 857 to Union Carbide Corporation, 1976.
[3] D.R. Fahey, J. Am. Chem. Soc. 103 (1981) 136.
[4] K. Ivanov, Appl. Catal., A 116 (1994) L1.
[5] J.M. Tatibouet, Appl. Catal., A 148 (1997) 213.
[6] D.J. Loder, US Patent 2 152 852 to E. I. du Pont de Nemours & Co., 1939.
[7] D.E. Hendriksen, Prepr. Pap. – Am. Chem. Soc., Div. Fuel Chem. 28 (1983) 176.
[8] H.J. Schmidt, H.J. Arpe, US Patent 4 501 917 to Hoechst AG, 1985.
[9] S.Y. Lee, J.C. Kim, J.S. Lee, Y.G. Kim, Ind. Eng. Chem. Res. 32 (1993) 253.
[10] D. He, W. Huang, J. Liu, Q. Zhu, Catal. Today 51 (1999) 127.
[11] T. Li, Y. Souma, Q. Xu, Catal. Today 111 (2006) 288.
[12] F.E. Celik, H. Lawrence, A.T. Bell, J. Mol. Catal. A: Chem. 288 (2008) 87.
[13] F.E. Celik, T. Kim, A.T. Bell, Angew. Chem. Int. Ed. 48 (2009) 4813.
[14] F.E. Celik, T. Kim, A.T. Bell, J. Catal. 270 (2010) 185.
[15] V. Shapovalov, A.T. Bell, J. Phys. Chem. C, submitted for publication.
[16] K.A. Koyano, T. Tatsumi, Micropor. Mater. 10 (1997) 259.
[17] J.F. Joly, N. Zanier-Szydlowski, S. Colin, F. Raatz, J. Saussey, J.C. Lavalley, Catal. Today 9 (1991) 31.
[18] L.Q. Xu, V.L. Zholobenko, L.M. Kustov, W.M.H. Sachtler, J. Mol. Catal. 83 (1993) 391.
[19] K. Nukada, Spectrochim. Acta 18 (1962) 745.
[20] M. Makarova, J. Dwyer, J. Phys. Chem. 97 (1993) 6337.
[21] S.C.L. Dias, J.L. de Macedo, J.A. Dias, Phys. Chem. Chem. Phys. 5 (2003) 5574.
[22] W. Lutz, C.H. Rüscher, D. Heidemann, Micropor. Mesopor. Mater. 55 (2002) 193.
[23] K. Schröder, J. Sauer, J. Phys. Chem. 100 (1996) 11043.
[24] Y. Kanazawa, K. Nukada, Bull. Chem. Soc. Jpn. 35 (1962) 612.
[25] T.R. Forester, R.F. Howe, J. Am. Chem. Soc. 109 (1987) 5076.
[26] H. Susi, T. Zell, Spectrochim. Acta 19 (1963) 1933.
[27] G.J. Millar, C.H. Rochester, K.C. Waugh, J. Chem. Soc. Faraday Trans. 87 (1991) 2785.
[28] ChemExper chemical directory, Methyl methoxyacetate. http://www.chemexper. com/search/cas/6290499.html (accessed 05.03.10).
[29] C. Chuang, W. Wu, M. Huang, I. Huang, J. Lin, J. Catal. 185 (1999) 423.
[30] S.M. Campbell, X. Jiang, R.F. Howe, Micropor. Mesopor. Mater. 29 (1999) 91.
[31] L. Kubelková, J. Nováková, K. Nedomová, J. Catal. 124 (1990) 441.
[32] Y.J. Jiang, M. Hunger, W. Wang, J. Am. Chem. Soc. 128 (2006) 11679.
[33] T.M. Duncan, R.W. Vaughan, J. Catal. 67 (1981) 49.
[34] T.M. Duncan, R.W. Vaughan, J. Catal. 67 (1981) 469.
[35] K. Hirota, K. Fueki, K. Shindo, Y. Nakai, Bull. Chem. Soc. Jpn. 32 (1959) 1261.
[36] B. Su, V. Norberg, C. Hansenne, Langmuir 16 (2000) 1132.
[37] NIST Chemistry WebBook, NIST Standard Reference Database Number 69 National Institute of Standards and Technology, Gaithersburg, MD. <http://www.webbook.nist.gov> (retrieved 18.04.10).
[38] P.S. Kalsi, Stereochemistry Conformation and Mechanism, New Age International, New Delhi, 2005.
[39] M. Jones Jr., Organic Chemistry, W.W. Norton & Company, New York, 1997.
[40] T.W.G. Solomons, Organic Chemistry, sixth ed., John Wiley & Sons, New York, 1996.
[41] S.J. Lombardo, A.T. Bell, Surf. Sci. Rep. 13 (1991) 1.
[42] V.P. Zhdanov, J. Pavlicek, Z. Knot, Catal. Rev. – Sci. Eng. 30 (1988) 501.
[43] Y. Zhao, D.G. Truhlar, Org. Lett. 8 (2006) 5753.
[44] Y. Zhao, D.G. Truhlar, J. Phys. Chem. C 112 (2008) 6860.
[45] Y. Zhao, N.E. Schultz, D.G. Truhlar, J. Chem. Theory Comput. 2 (2006) 364.
[46] Y. Zhao, D.G. Truhlar, Acc. Chem. Res. 41 (2008) 157.
[47] N. Hansen, T. Kerber, J. Sauer, A.T. Bell, F.J. Keil, J. Am. Chem. Soc., accepted for publication.